SF 298 MASTER COPY KEEP THIS COPY FOR REPRODUCTION PURPOSES

REPORT DOCUMENTATION PAGE

Form Approved
OMB NO. 0704-0188

1. AGENCY USE ONLY *(Leave blank)*	2. REPORT DATE	3. REPORT TYPE AND DATES COVERED
		FINAL PROGRESS REPORT 6/20/95 - 12/19/96

4. TITLE AND SUBTITLE

Spatial, Spectral and Temporal-Resolved Scanning Optical Microscope

5. FUNDING NUMBERS

DAAH04-95-1-0380

6. AUTHOR(S)

Hans D. Hallen, Boris I. Yakobson

7. PERFORMING ORGANIZATION NAMES(S) AND ADDRESS(ES)

North Carolina State University
Department of Physics
Raleigh, NC 27695-8202

8. PERFORMING ORGANIZATION REPORT NUMBER

9. SPONSORING / MONITORING AGENCY NAME(S) AND ADDRESS(ES)

U.S. Army Research Office
P.O. Box 12211
Research Triangle Park, NC 27709-2211

10. SPONSORING / MONITORING AGENCY REPORT NUMBER

ARO 34750.1-PH-RIP

11. SUPPLEMENTARY NOTES

The views, opinions and/or findings contained in this report are those of the author(s) and should not be construed as an official Department of the Army position, policy or decision, unless so designated by other documentation.

12a. DISTRIBUTION / AVAILABILITY STATEMENT

Approved for public release; distribution unlimited.

12 b. DISTRIBUTION CODE

19970226 037

13. ABSTRACT *(Maximum 200 words)*

This instrumentation development project has made considerable progress towards its goals of producing a near field scanning optical microscope which tests the limits of spatial, temporal and spectral resolution, and which utilizes probes designed for optimal throughput and minimal probe heating. Specifically, (i) a Ti-sapphire laser has been constructed and successfully mode-locked with fsec-scale pulses, (ii) a Raman detection system using a cooled CCD detector and a holographic filter has been configured, and (iii) several near-field instrument heads and electronics sub-systems built. The microscopes feature a novel constant linear motion coarse approach and improved probe-sample distance detection scheme developed under this project. A computer workstation has been purchased and programmed to (iv) model the images from the instrument in its time-resolved excess carrier studies mode, and to (v) perform ray tracing which has been used to suggest a novel rational probe design. Efforts are underway which utilize the instrument for sub psec time-resolved studies of excess carriers in silicon and to study near-field effects in Raman spectroscopy of KTP samples.

14. SUBJECT TERMS

Near Field Scanning Optical Microscopy, Instrument Design
Pump-Probe Techniques, Temporal Resolution

15. NUMBER IF PAGES

10 pages

16. PRICE CODE

17. SECURITY CLASSIFICATION OR REPORT	18. SECURITY CLASSIFICATION OF THIS PAGE	19. SECURITY CLASSIFICATION OF ABSTRACT	20. LIMITATION OF ABSTRACT
UNCLASSIFIED	UNCLASSIFIED	UNCLASSIFIED	UL

NSN 7540-01-280-5500

Enclosure 1

Standard Form 298 (Rev. 2-89)
Prescribed by ANSI Std. 239-18
298-102

GENERAL INSTRUCTIONS FOR COMPLETING SF 298

The Report Documentation Page (RDP) is used in announcing and cataloging reports. It is important that this information be consistent with the rest of the report, particularly the cover and title page. instructions for filling in each block of the form follow. It is important to ***stay within the lines*** to meet ***optical scanning requirements.***

Block 1. Agency Use Only *(Leave blank)*

Block 2. Report Date. Full publication date including day, month, and year, if available (e.g. 1 Jan 88). Must cite at least year.

Block 3. Type of Report and Dates Covered. State whether report is interim, final, etc. If applicable, enter inclusive report dates (e.g. 10 Jun 87 - 30 Jun 88).

Block 4. Title and Subtitle. A title is taken from the part of the report that provides the most meaningful and complete information. When a report is prepared in more than one volume, repeat the primary title, add volume number, and include subtitle for the specific volume. On classified documents enter the title classification in parentheses.

Block 5. Funding Numbers. To include contract and grant numbers; may include program element number(s), project number(s), task number(s), and work unit number(s). Use the following labels:

C	- Contract	**PR**	- Project
G	- Grant	**TA**	- Task
PE	- Program Element	**WU**	- Work Unit Accession No.

Block 6. Author(s). Name(s) of person(s) responsible for writing the report, performing the research, or credited with the content of the report. If editor or compiler, this should follow the name(s).

Block 7. Performing Organization Name(s) and Address(es). Self-explanatory.

Block 8. Performing Organization Report Number. Enter the unique alphanumeric report number(s) assigned by the organization performing the report.

Block 9. Sponsoring/Monitoring Agency Name(s) and Address(es). Self-explanatory.

Block 10. Sponsoring/Monitoring Agency Report Number. *(If known)*

Block 11. Supplementary Notes. Enter information not included elsewhere such as; prepared in cooperation with...; Trans. of...; To be published in.... When a report is revised, include a statement whether the new report supersedes or supplements the older report.

Block 12a. Distribution/Availability Statement. Denotes public availability or limitations. Cite any availability to the public. Enter additional limitations or special markings in all capitals (e.g. NORFORN, REL, ITAR).

DOD	- See DoDD 4230.25, "Distribution Statements on Technical Documents."
DOE	- See authorities.
NASA	- See Handbook NHB 2200.2.
NTIS	- Leave blank.

Block 12b. Distribution Code.

DOD	- Leave blank
DOE	- Enter DOE distribution categories from the Standard Distribution for Unclassified Scientific and Technical Reports
NASA	- Leave blank.
NTIS	- Leave blank.

Block 13. Abstract. Include a brief *(Maximum 200 words)* factual summary of the most significant information contained in the report.

Block 14. Subject Terms. Keywords or phrases identifying major subjects in the report.

Block 15. Number of Pages. Enter the total number of pages.

Block 16. Price Code. Enter appropriate price code *(NTIS only).*

Block 17. - 19. Security Classifications. Self-explanatory. Enter U.S. Security Classification in accordance with U.S. Security Regulations (i.e., UNCLASSIFIED). If form contains classified information, stamp classification on the top and bottom of the page.

Block 20. Limitation of Abstract. This block must be completed to assign a limitation to the abstract. Enter either UL (unlimited) or SAR (same as report). An entry in this block is necessary if the abstract is to be limited. If blank, the abstract is assumed to be unlimited.

SPATIAL, SPECTRAL AND TEMPORAL-RESOLVED SCANNING OPTICAL MICROSCOPE

FINAL PROGRESS REPORT

Hans D. Hallen, Boris I. Yakobson

February 17, 1997

U.S. ARMY RESEARCH OFFICE

CONTRACT/GRANT NUMBER DAAH04-95-1-0380

NORTH CAROLINA STATE UNIVERSITY

FORWARD

Fast, sharp, and colorful images are characterized by the measured sample response time Δt, the size of resolved features Δx, and the signal spectral resolution $\Delta\omega$. These "3Δ" define a three-dimensional space in optical imaging. In this framework, advances in imaging science may be made on several fronts, i.e. toward smaller Δt, Δx, or/and $\Delta\omega$. Many of the most powerful modern methods of *temporal* optical measurement rely on the use of high peak power picosecond and femtosecond laser techniques, thus achieving $\Delta t < 10^{-12}$ s. These include the measurement of electron dynamics on the femtosecond or longer time scales and a host of new nonlinear optical investigations, using techniques such as spectroscopy and selective (e.g. defect) imaging. Similarly, the near-field scanning optical microscope (NSOM) incorporates a rapidly evolving approach to increase the *spatial* resolution of optical measurements beyond the diffraction limit. Conventional optical instruments provide optical probes no smaller than $\lambda/2$, whereas the limit to NSOM resolution depends upon the size of a physical aperture. *Spectral* resolution has been demonstrated in a number of NSOM studies, with most current work focused on exploitation of relative weak spectral signatures.

NSOM has been used in several contrast modes including polarization [1] in both transmission and reflection and through the transduction of magnetic- [2], spectroscopic- [3-5], fluorescence- [6], and time-resolved images on both the μsec [7-9] and the nanosec [10] timescales. Overall, one still can say that the NSOM development has mostly been driven by desire to achieve as small Δx as possible. Although the ultimate NSOM spatial resolution may not yet be a matter of consensus, a material limit on the order of 12 nm for green light is generally accepted. At this current level of instrument maturity, some of the most exciting challenges in NSOM development involve incorporation of multiple contrast mechanisms into one microscope.

It is useful at this point to consider what kinds of simultaneous temporal, spatial, and spectroscopic resolution can be achieved. The energy-time uncertainty principle limits the combined temporal and spectral resolution, and can be reached in some ultrafast studies. Spatial resolution does not present such a hard or straightforward barrier. Rather the signal intensity decreases rapidly as a function of the resolution divided by the wavelength. One must then take into account statistical and electronic noise to determine if a signal can be identified within some time duration, i.e., we must define an averaging time Δt_{ave}. This averaging time may be less than our temporal resolution Δt, as in 1-shot acquisition, or it may be significantly longer if the process is made to repeat itself while averaging is performed. The maximum Δt_{ave} may be limited by either the desirable time sampling interval (e.g., in video-rate imaging) or by the instrument stability (e.g., in NSOM-Raman imaging), whichever is more restrictive. The choice of Δt_{ave} depends upon the probe in terms of the number of photons/second it delivers (includes Δx), the experimental cross section for the process under study, the collection efficiency, the time interval (time resolution), and the wavelength interval (spectral resolution). We do not quantify these here, but note that only two major variables can be optimized without affecting the data quality. These are: the maximum allowed Δt_{ave} and the amount of light output from the probe for a given Δx (or, generally more restrictive, for the whole triad $\{\Delta x, \Delta t, \Delta\omega\}$). We are actively working in both arenas, i.e. we are striving to enhance the stability of the microscope head [11] (to increase the signal averaging time) and to optimize light coupling through the optical probe (to increase light output).

STATEMENT OF THE PROBLEM STUDIED

The object of this instrument development project is the development of a near-field optical microscope (NSOM) capable of simultaneously providing spatial, temporal and spectral resolution. While parallel detection of such information is straightforward in conventional optical imaging, the light-delivery inefficiency of the sensing element in an NSOM - usually a coated tapered optical fiber - puts severe limitations on the available signal in near-field microscopy and spectroscopy. This limit presents special challenges in near-field optical studies. Our instrument overcomes these challenges by using

NSOMs with a rigid, low-drift design which was developed under previous ARO funding [11] and enhanced under this project. [12] Spectral contrast in imaging is obtained through analysis of the signal scattered from the sample, with a dedicated Jarrell-Ash Raman spectrometer which was provided for the project by the University. Temporal resolution is provided by a pulsed laser source. Funding levels required that this source, a Ti-sapphire laser operating in a self mode-locked configuration, be machined, constructed and aligned as part of the project. Critical to the development of the proposed multi-faceted NSOM are improvements in probe design and fabrication. These latter efforts to improve the tapered fiber probe -- the heart of NSOM and the source of the signal-to-noise problems -- have included theoretical modeling of light propagation in the probe and experimental studies. We have made some progress towards transforming the commonly-used empirical "recipe" approach into a rational design for tip fabrication. Modeling of the image contrast in NSOM is also an issue, since the length scales are so small that common thinking can begin to fail. Efforts in modeling the contrast in time-resolved images of excess carriers in silicon has developed significantly during this project, and the combined measurements and models have drawn interest from several companies, including KLA Instruments, Micron Technology, and Westinghouse Electric Corporation.

The industrial and scientific interest in our time-resolved NSOM work stems from its ability to map defects in semiconductors with very high spatial resolution, and the new regime for studying conduction which is made available by the combination of time and space localization. The latter refers to the fact that scattering lengths for electrons in silicon are typically a few hundred nanometers, while the resolution of the NSOM instrument is smaller. Thus, one can study the pre-diffusive behavior of the charge carriers if the time resolution is fast enough so that observations occur before a diffusion profile accumulates. This is now possible with the instrument constructed during this project using pulses of visible and near-infrared light. The former point of interest, the defect mapping abilities, were developed during earlier ARO-funded work were the first to use two-wavelength pumping/monitoring with NSOM, for local excess carrier lifetime measurements. [7-9, 13-16] The industrial interest in those results provided incentive to both develop them further and to explore related methods which could be measured faster (the recombination time in silicon is rather slow -- msec for good material -- necessitating long delays at each point). This instrument provides the core for such a related method, by directly observing scattering in the pre-diffusive regime with pulses of light having different wavelengths. Evidence for the diffusive process was observed in our earlier work and is presented in figure 1. The data at low frequencies is dominated by carrier lifetime effects, the data does not become zero at higher frequencies, which is indicative of another, faster,

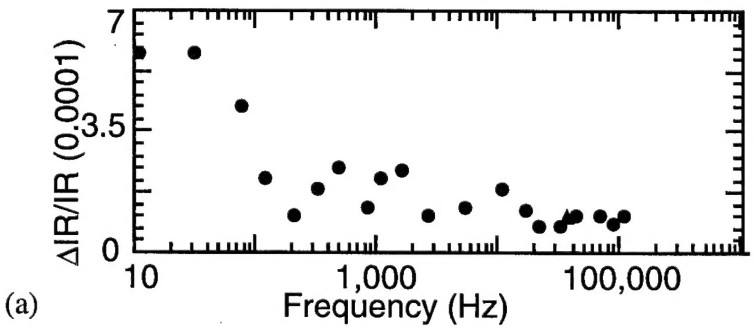

(a)

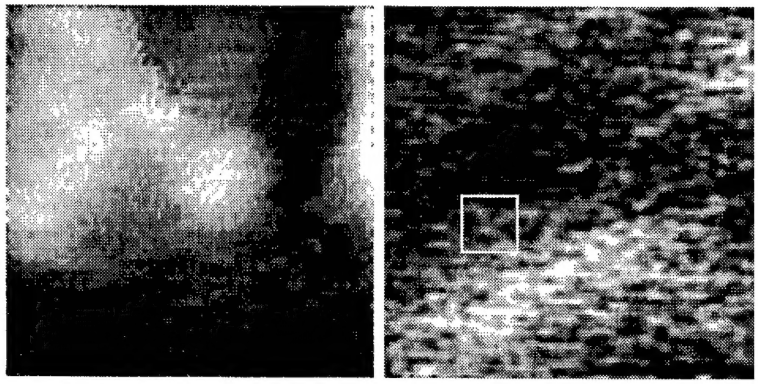

(b) (c)

Figure 1: (a) A plot of the relative IR signal change vs. the visible light switching frequency reflects the response of the excess carriers, with lifetime (at knee) of 1.6 msec. (b)-(c) 7.5 μm square images of the IR signal change at visible light is switching frequencies of (b) 100 Hz and (c) 20 kHz, illustrate where lifetime and diffusion dominate. The box in (c) is one wavelength (of 1.15 μm IR) square.

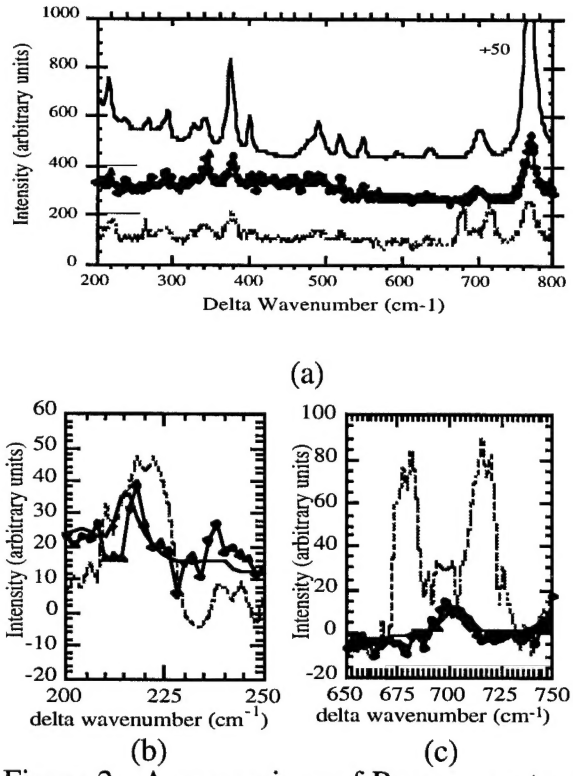

Figure 2. A comparison of Raman spectra in the near-field vs. the far-field for a KTP sample. (a) The overview: the top (solid) curve is a microRaman spectrum while the lower two are obtained through a fiber probe not in (middle, with points) and in (bottom, dashed) the near-field of the sample, note the shifted baselines on the left. (b,c) Portions of the spectra in (a) after scaling to overlay the large peak at 767 cm-1. The larger and shifted peak in the near-field data of (b) is due to an extra vibration mode which can be coupled to with longitudinally polarized light. The large split peaks in (c) cannot be explained by changes in coupling to modes, but is attributed to surface stresses and surface enhancement in the near-field.

serial process which is diffusion in this case. Since it is a faster process, its effects can be noticed on shorter time scales, so the data can be acquired faster as is required for modern optical diagnostics on semiconductors. This will form one of the core uses of the instrument. Both measurements require similar instruments, thus this aspect of the project focused on providing an instrument with short pulses of light at two wavelengths.

Our Army Research Office funded efforts in Raman spectroscopic imaging have proven that NSOM Raman spectroscopy and imaging are possible. [3-5] They have also revealed several important differences from standard far-field Raman spectroscopy. [17] These include (i) concurrent and independent topographic imaging, (ii) surface enhancement, (iii) selection rule variation due to the presence of significant amounts of longitudinally polarized light, (iv) reduction in the Rayleigh tail due to the small sampled volume, and (v) spatial resolution. It was also found that the quality of the probe used in illumination mode could be deduced from the signal from the silica within the probe itself: the smaller the silica peak, the better the probe. Figure 2 shows a comparison between a conventional far-field microRaman spectrum, an NSOM Raman spectrum with the aperture brought away from the surface, and an NSOM Raman spectrum with the probe held in the near field. The spectrum through the NSOM aperture held in the far-field resembles the microRaman spectrum as it should. The near-field NSOM spectrum shows the properties noted above. The analysis is based upon the identification of mode symmetries and comparison of the near-field and far-field spectra. Although we have identified these differences using a time-intensive serial detection scheme, we were not able to study the effects in detail. The problem undertaken with this project to resolve the situation was to design a parallel detection scheme for Raman measurements while maintaining the thermal stability attained previously. This permits the careful measurements now underway to study the novel NSOM-Raman effects in detail.

Many spectroscopic studies are hindered by the small amount of light which passes through an NSOM probe. We had studied this in detail for existing probe designs in previous ARO-funded efforts. [18] The problem is that the geometry of the probe must restrict the amount of light it passes, and the rejected energy heats the probe tip to the point of failure. An example is shown in figure 3. The probe is shown in (a) using an external light source, which is turned off in (b) to reveal a viewing optics limited spot of light emanated (and quickly diffracted into all directions) from the tip. After the intensity of light was increased to ~10mW for a short time, the probe was destroyed as is evident in (c) which shows light scattered from the probe several microns behind the former aperture. Although our previous work had been able to qualitatively explain the damage process (d), a fundamental solution to the problem was not

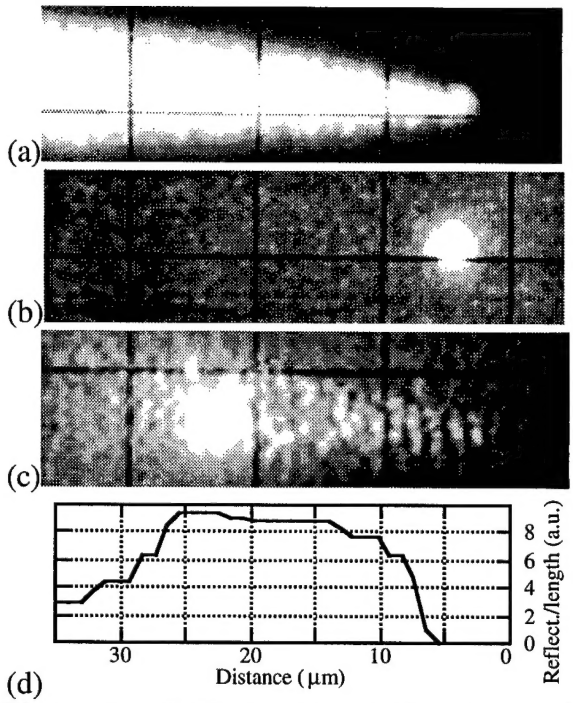

Figure 3: Optical micrographs of a probe illustrate a typical (a) probe shape as viewed by external illumination, (b) optical emission of the same new aluminum coated probe from a point at the end, and (c) the optical emission of the same probe after damage by coupling 14 mW of green light into the probe. The scale of the dark grids in the micrographs is 10 μm per box. For comparison, the results of a ray tracing model which counts the number of ray bounces per length is shown in (d).

found. The problem undertaken in this aspect of the project was to identify a better probe shape or construction which would dissipate less energy near the probe, alleviating the detrimental heating. This involved efforts at adjusting both the shape of the probe and the location of the opaque metal layer used to form the aperture.

SUMMARY OF THE MOST IMPORTANT RESULTS

This instrumentation development project has made considerable progress towards its goals of producing a near field scanning optical microscope which tests the limits of spatial, temporal and spectral resolution, and which utilizes probes designed for optimal throughput and minimal probe heating. Specifically, (i) a Ti-sapphire laser has been constructed and successfully mode-locked with fsec-scale pulses, (ii) a Raman detection system using a cooled CCD detector and a holographic filter has been configured, and (iii) several near-field instrument heads and electronics sub-systems built. The microscopes feature a novel constant linear motion coarse approach and improved probe-sample distance detection scheme developed under this project. A computer workstation has been purchased and programmed to (iv) model the images from the instrument in its time-resolved excess carrier studies mode, and to (v) perform ray tracing which has been used to suggest a novel rational probe design. The workstation has also been used for (vi) modeling carbon nanotubes, with the results being widely circulated by the popular press. Efforts are underway which utilize the instrument for sub-psec time-resolved studies of excess carriers in silicon and to study near-field effects in Raman spectroscopy of KTP samples. We will consider each of these accomplishments in more detail.

(i) Temporal resolution, the pulsed laser source.

The Ti-sapphire laser constructed for this project was based upon the 'standard' University of Washington design, [19, 20] with modifications by the ARO group of Henry Everitt at Duke. This laser was pumped by an Ar ion laser purchased with grant money, but the University supplied a trade-in laser for reduced cost. The laser is now operational. Of note in the arduous task of aligning the laser to self mode-lock is a recent paper which gives an estimate of the positions of the focusing cavity mirrors relative to the crystal. [21] We have developed an alignment procedure which is available on request. A fast oscilloscope trace can indicate that mode-locking is occurring, and allow an estimate of the ratio of mode-locked energy to that in a concurrent continuous wave oscillation. Such a trace is shown in figure 4, where the time between pulses reflect the time for light to travel twice the cavity length, giving a frequency of 80 MHz for our laser, but the pulse shape is dominated by the electrical characteristics of the photodiode, cabling, and input amplifiers of the oscilloscope and not the optical pulse. One can estimate the true pulse duration by interfering part of a pulse with itself in a Michelson configuration, or more simply (and coarsely) by use of the Heisenburg energy-time uncertainty relation, which relates the energy spread to a minimum duration. The wavelength smear in figure 4 taken during the optimization

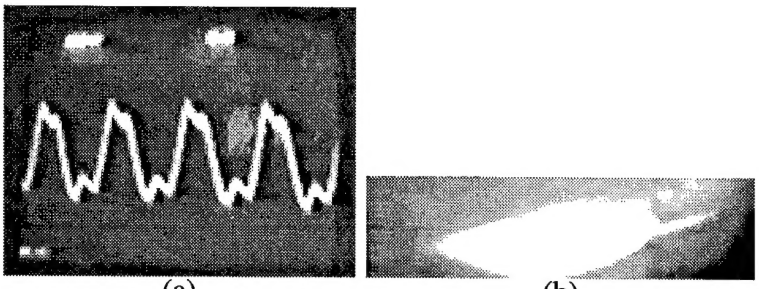

(a) (b)

Figure 4: (a) An oscilloscope trace of a photodiode output shows the optical pulse train from the Ti-sapphire laser, total trace length is 50 ns. (b) The wavelength spread of the laser output after reflecting from a grating. The smear is centered about 810nm and has a range +/-12nm. The average output power was about 200mW

for mode-locking shows a wavelength range of ~25 nm at ~800 nm which gives a limit that the pulse is longer than 15 fsec. We expect it is in the 30-100 fsec range.

(ii) Spectral resolution, adaptation of the Raman spectrometer.

The signal levels with current NSOM probes give ~10 photons/second for a few wavenumber wide bin in Raman spectroscopy of a material with a fairly strong Raman cross section. For adequate signal to noise ratio, 20-30 second averaging times are required per point. Spectroscopy with the photon-counting photomultiplier tubes used in the past required a separate integration time for each point, or ~2 hours/spectrum. [17] Imaging times were ~10 hours/image at a single wavelength. [3, 4] To help reduce the time needed for NSOM-Raman spectroscopy, this aspect of the project, spectral resolution, focused on optimizing parallel detection. A CCD detector was mounted at the output of the first stage of a double 1 meter Czerney-Turner spectrometer. The second stage was not used so that the system would have a higher throughput. Unscattered light was further rejected with a holographic filter placed before the spectrometer input. A 2-stage cooled CCD camera was chosen as a compromise between cost and performance, and should provide similar noise performance to the photomultiplier tube while providing parallel detection. We note that although the instrument can detect a spectrum in parallel and therefore reduce the spectrum acquisition time to a single averaging time of 10-30 sec, imaging times will still measure in the hours. This is because the NSOM only illuminates one image point at a time, so each point must still be averaged independently. Much more information results from such an image, however, since a complete spectrum results at each image point. In many situations we expect to need Raman spectra only at a few points in the image rather than at every point, with another contrast mechanism used to identify the proper location. In this case the Raman spectroscopy would not significantly increase the imaging time beyond the few minutes per image typical with fraction-of-a-second averaging times per pixel typical in NSOM systems.

(iii) Novel aspects of the NSOM.

One of the reliability problem areas for NSOM instruments has been the probe to sample distance regulation system. We have addressed this problem in this project by modifying a novel design by Julia Hsu's group at the University of Virginia. [22] We improved the signal to noise ratio, and eliminated the need to dedicate an expensive lock-in amplifier for the distance regulation subsystem. This work has been submitted for publication in the Review of Scientific Instruments. [12] The technique involves the measurement of the impedance of a piezoelectric element driving the probe at resonance. As the probe interacts with the sample, a force is generated at the resonant frequency. This effects the impedance of the piezo, which is detected in a bridge configuration. The current induced by the driving voltage is compared to a phase-shifted copy of the drive voltage, and the difference amplified, filtered, and converted from the resonant frequency ~50 kHz to low frequencies in a commercial RMS converter chip. This output is tuned to zero with a retracted probe, and its offset from zero used to drive a feedback circuit. This scheme seems to greatly improve reliability and provide consistent low noise topographic images.

Another novel design aspect of the NSOM instrument is the coarse positioning system. The aim is to provide a system which would work at a variety of temperatures and operational configurations while providing rapid engagement of the fine feedback system with no risk of probe crash. Our previous system met many of these constraints, [11] but did not operate at cryogenic temperatures, and was rather slow in approaching the surface since a search for the surface with the fine positioning was required between every few coarse positioning steps to insure the probe did not crash. This search was

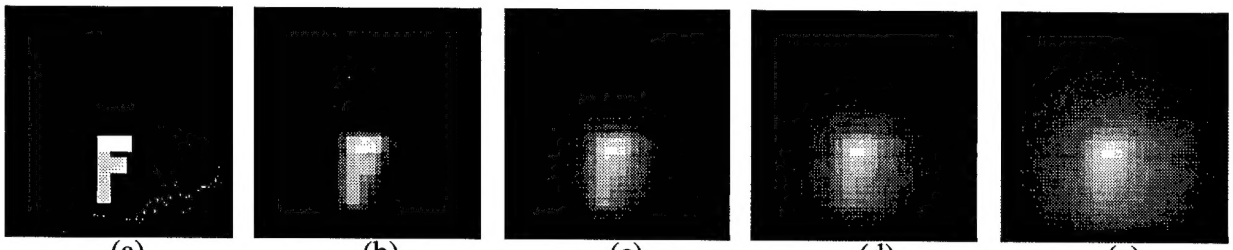

(a) (b) (c) (d) (e)

Figure 5. A sample of simulated infrared transmittance-images under the uniform illumination by a visible light. The carriers relaxation rate is 10-20 times faster within the F-letter than elsewhere. Their mobility, and relative scaling for the gray range varies from none, 1 (a), to 0.02D, 1.05 (b), to 0.1D, 1.3 (c) to 0.25D, 1.7 (d), and D, 3.2 at (e). The background lifetime of 1 μs and the frame size of 10 μm would correspond to D = 1 cm^2/s.

necessitated by the sharp inward lunge of the tip and subsequent relaxation away in the inertial sliding motion used. The constant linear motion system invented during this project is smooth enough that no fine positioning search is required, greatly speeding the approach process. Further, we expect a much wider operating temperature range, including motion at cryogenic temperatures.

(iv) Temporal resolution, modeling the image contrast.

This can be illustrated by the computer simulation, which also allows us to consider more complex geometries of defect domains. The excess carrier population $n(\mathbf{x},t)$ created by the visible light pump is governed by the kinetic equation [7]

$$\partial n(\mathbf{x},t)/\partial t = q \cdot P(\mathbf{x},t) + \iiint T(\mathbf{x},\mathbf{x}') \cdot n(\mathbf{x}',t) \cdot d^3\mathbf{x}' - n(\mathbf{x},t) / \tau(\mathbf{x}), \qquad (3)$$

where the first term is the rate of generation by the pump-probe, the second describes the transport of carriers and the third one represents the local lifetime $\tau(\mathbf{x})$. $P(\mathbf{x},t)$ is the density of illumination power, and q is the quantum yield for the visible light. The absorption of the infrared component, due to local concentration $n(\mathbf{x},t)$, is then proportional to the spatial convolution in the vicinity of the probe aperture, $A(\mathbf{x_o}) = \int_a A(\mathbf{x_o},\mathbf{x}) \cdot n(\mathbf{x},t) \cdot d^3\mathbf{x}'$. If the mean-free-path is shorter than the length-scale of interest (e.g. the resolution claimed) then the transport integral reduces to the usual diffusion term *div* [$D(\mathbf{x})$ *grad* $n(\mathbf{x},t)$]. Imaging $n(\mathbf{x},t)$ with NSOM probe gives information about lifetime variations due to variations in defect concentration. Generally, however, the picture is largely smeared by the motion of carriers. Assuming a certain model defect distribution, the solution of this equation allows a simulation of the carrier evolution and a calculation of the probe-collected signal for every pixel at different locations across the sample. Fig. 5 presents the IR-transparency under steady and uniform illumination by visible light. [8] The feature to be imaged is characterized by 10-20 times shorter local lifetime, and is shaped as the letter "F". As one could expect, the higher mobility of carriers results in a less distinct image. Nevertheless, the signal profiling allows an unambiguous extraction of a diameter for the defect-filled domain. A less trivial observation is that the internal details of the imaged structure appear to be lost and can not be restored by a simple contrast enhancement: the more than three times greater contrast in fig. 5e still does not allow identification the written-in pattern.

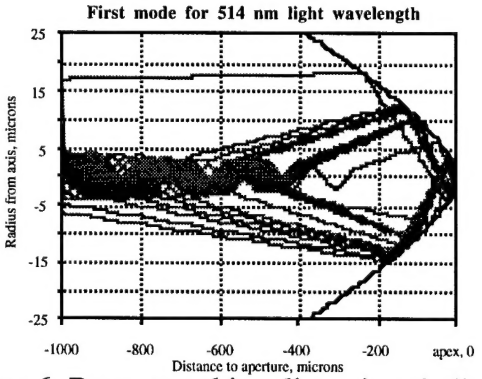

Figure 6: Rays traced in a linear/parabolic tip. The density of bounces along the surface is related to the sideput density.

(v) Probe design, ray tracing results.

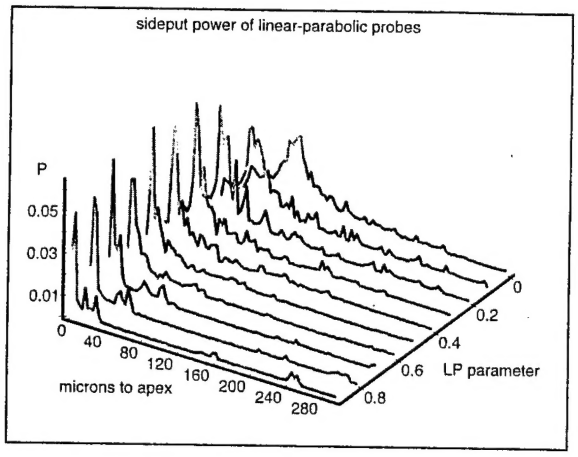

Figure 7: The sideput, or number of ray bounces (energy loss) per length, is shown for a family of probes which vary from nearly parabolic (LP = 0) to nearly linear.

Our theoretical effort was aimed at determining if improvements could be made in taper shape. It was based on the ray-tracing through the tapers of different shapes (Fig. 6) [23] In characterizing taper shape in terms of a gradual transition between a linear (conical) and a parabolic (parabolic of revolution) taper, we calculated the produced sideput density for shapes between these two extremes. Show in figure 7 is the side-put density for a family of ten such tapers. Notable in these curves is the decrease in sideput density at distances far removed from the taper apex for the most parabolic tapers (LP=0). Surprisingly, the vast majority of the interactions of the light with the glass interface take place at angles sufficiently glancing so as to result in TIR in the absence of a metal coating. Since the metal is responsible for the breakdown of the fiber at high intensities, a novel structure now seems obvious. A taper with only an annulus of metal at its apex would be much more robust than a fully coated taper. We have initiated a program designed at fabricating such a probe.

(vi) Modeling carbon nanotubes.

In an effort not directly related with the current NSOM research, but important for the possible future innovations of the probe microscopy, we have studied the properties of carbon nanotubes. [24, 25] In particular, their mechanics, response to compression, torsion, bending, and the strength. In this project part of the simulations and visualization was performed on the SGI work station, obtained with the ARO funding of this project. The work was featured worldwide, as one of the examples (from the Sci. Comp. World magazine) illustrates here, Fig. 8.

Figure 8: An example of the carbon nano-tube studies from the popular press.

Simulations show high strength of nanotubes

Carbon fullerene "nanotubes" are extremely strong, according to recent simulations of their mechanical behaviour. Researchers at North Carolina State University (NCSU) in the USA examined the energy profiles of the hollow molecules under compressional, torsional and flexural stress. They found that the nanotubes could sustain very large local strains without any bond breaking or switching.

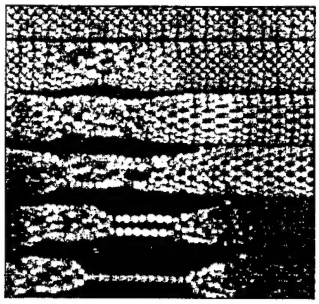

Temporal sequence of nanotube fracture (37% strain).

Under axial tension, the nanotubes can theoretically sustain loads of up to 200 GPa – equivalent to supporting a 20 tonne load on a filament just 1 mm in diameter. Under stress their behaviour was consistent with the continuous tubule model. The nanotube had a Young's modulus of 5.5 TPa and could be stretched by up to 40% without breaking.

Nanotubes are members of the fullerene family, which also includes the carbon-60 "buckyball". The simulations have corroborated recent experimental studies of nanotubes using transmission electron microscopy, which have shown that greatly distorted configurations are possible without any atomic defects in the nanotube structure.

The simulations performed at NCSU were based on the recent development of many-body interatomic potentials. Simulations were run on IBM RS/6000 and Silicon Graphics Indigo computers using in-house molecular dynamics software. The work has excited interest in the possible applications of high-strength nanotube wires. □

LIST OF MANUSCRIPTS SUBMITTED OR PUBLISHED UNDER ARO SPONSORSHIP DURING THIS PROJECT, INCLUDING JOURNAL REFERENCES:

Refereed Journals

i. "A Shear Force Feedback Control System for Near-field Scanning Optical Microscopes without Lock-in Detection," J. W. P. Hsu, A. A. McDaniel, and H. D. Hallen, submitted to Rev. Sci. Instr.

ii. "Structural mechanics of carbon nanotubes: From continuum elasticity to atomistic fracture," B. I. Yakobson, C. J. Brabec and J. Bernholc, J. of Computer-Aided Design **3**, 173 (1996).

iii. "Optical imaging of carrier dynamics with sub-wavelength resolution," A. LaRosa, B. I. Yakobson, H.D. Hallen, Appl. Phys. Lett, (in press).

iv. "A versatile, stable scanning proximal probe microscope," C.L. Jahncke and H.D. Hallen, Review of Scientific Instruments, (in press).

v. "Thermal/optical effects in NSOM probes," B. I. Yakobson, A. LaRosa, H.D. Hallen, and M. A. Paesler, Ultramicroscopy, **59**, 334 (1995).

vi. "Nano-raman spectroscopy and imaging with the near-field scanning optical microscope," C.L. Jahncke, H.D. Hallen, and M. A. Paesler, An invited contribution to the J. Raman Spectroscopy, **27**, 579-586 (1996).

vii. "Origins and effects of thermal processes in near-field optical probes," A. LaRosa, B. I. Yakobson, and H.D. Hallen, Appl. Phys. Lett. **67**, (18), 2597-2599 (1995).

viii. "Raman imaging with near-field scanning optical microscopy," C.L. Jahncke, M. A. Paesler, and H.D. Hallen, Appl. Phys. Lett. **67**, (17), 2483-2485 (1995).

Conference Proceedings

i. C.L. Jahncke and H.D. Hallen, "Near-field Raman Spectra: surface enhancement, z-polarization, fiber Raman background and Rayleigh scattering," Proceedings of LEOS (1996).

ii. "Energy Dissipation in NSOM Probe Fiber Tapers: Ray Tracing Assessment," P. O. Boykin, M. A. Paesler, B. I. Yakobson, Proceedings of Biomedical Fiber Optics, SPIE **2677**, 148-153 (1996).

iii. "Imaging of silicon carrier dynamics with Near-field Scanning Optical Microscopy", A. H. La Rosa, B. I. Yakobson and H. D. Hallen, Mat. Res. Soc. Symp. Proc. Vol. **406**, pp.189-194 (1996).

iv. "Thermal/temporal response of the NSOM probe/sample system," H.D. Hallen, B. I. Yakobson, A. LaRosa, and M. A. Paesler, SPIE Proceedings **2535**, 34-37 (1995).

LIST OF ALL PARTICIPATING SCIENTIFIC PERSONNEL SHOWING ANY ADVANCED DEGREES EARNED BY THEM WHILE EMPLOYED BY THIS PROJECT

Faculty Participants: Hans D. Hallen, Boris I. Yakobson
Michael Paesler
Graduate Student Participants:
Andres La Rosa, graduated with Ph.D, June, 1996

Sean Boylan, M.S. candidate
Eric Ayars, Ph.D. candidate

REPORT OF INVENTIONS (BY TITLE ONLY)

i. "A variable temperature electrically driven constant velocity translator with nanometer-scale precision" was invented during this project and we are considering a patent disclosure statement.

BIBLIOGRAPHY

[1] P. Moyer and M.A. Paesler, Precision Engineering Center Annual Report **9**, 3 (1991).
[2] T.J. Silva and S. Schultz, Ultramicroscopy **57**, (1995).
[3] C.L. Jahncke, M.A. Paesler and H.D. Hallen, Appl. Phys. Lett. **67**, 2483 (1995).
[4] C.L. Jahncke and H.D. Hallen, Bull. Am. Phys. Soc. **40**, 685 (1995).
[5] C. L. Jahncke, H. D. Hallen and M. A. Paesler, J. of Raman Spectroscopy **27**, 579 (1996).
[6] Eric Betzig and Robert J. Chichester, Science **262**, 1422 (1993).
[7] A.H. LaRosa, B.I. Yakobson and H.D. Hallen, Appl. Phys. Lett., to appear 31 March 1997.
[8] A. H. LaRosa, B. I. Yakobson and H. D. Hallen, Proceedings of MRS Fall Meeting, Boston, Vol. **406**, pp.189-194 (1996).
[9] A. LaRosa, C.L. Jahncke and H.D. Hallen, Ultramicroscopy **57**, 303 (1995).
[10] X. Sunney Xie and Robert C. Dunn, Science **265**, 361 (1994).
[11] C.L. Jahncke and H.D. Hallen, Rev. Scient. Instr. in press (1996).
[12] J. W. P. Hsu, A. A. McDaniel and H. D. Hallen, Rev. Sci. Instr. (submitted).
[13] A.H. LaRosa, C.L. Jahncke and H.D. Hallen, SPIE Proceedings **2384**, 101 (1995).
[14] A. H. LaRosa, B. I. Yakobson, M. A. Paesler and H. D. Hallen, Proceedings of Proceedings of Conference on Near Field Optics and Related Techniques NFO-3, Brno, Czech Republic, Ultramicroscopy (1995).
[15] H.D. Hallen, B.I. Yakobson, A. LaRosa and M.A. Paesler, SPIE **2535**, 34 (1995).
[16] H. D. Hallen, A. H. La Rosa and C. L. Jahncke, Phys. Stat. Sol. (a) **152**, 257 (1995).
[17] C.L. Jahncke and H.D. Hallen, Proceedings of LEOS, (1996).
[18] A. H. LaRosa, B. I. Yakobson and H. D. Hallen, Appl. Phys. Lett. **67**, (1995).
[19] Melanie T. Asaki, Chung-Po Huang, Dennis Garvey, Jianping Zhou, Henry C. Kapteyn and Margaret M. Murmane, Optics Letters **18**, 977 (1993).
[20] Kendall Read, Florian Blonigen, Nicole Riccelli, Margaret Murmane and Henry Kapteyn, Optics Letters **21**, 489 (1996).
[21] Ivan P. Christov, Vency D. Stoev, Margaret M. Murmane and Henry C. Kapteyn, Optics Lett. **20**, 2111 (1995).
[22] J.W.P. Hsu, M. Lee and B.S. Deaver, Review of Scientific Instruments **66**, 3177 (1995).
[23] P.O. Boykin, M.A. Paesler and B.I. Yakobson, SPIE Proceedings **2677**, 148 (1996).
[24] B. I. Yakobson, C. J. Brabec and J. Bernholc, J. of Computer-Aided Design **3**, 173 (1996).
[25] B. I. Yakobson, C. J. Brabec and J. Bernholc, Phys. Rev. Lett. **76**, 2511 (1996).